Next Energy 7 (2025) 100216

Contents lists available at ScienceDirect

Next Energy

journal homepage: www.sciencedirect.com/journal/next-energy

Research article

Enhanced electrochemical performance of polycrystalline NCM811 cathode at high voltage through Te-doped $LiNbO_3$ coating for lithium-ion batteries

Mohamed M. Abdelaal, Mohammad Alkhedher*

Mechanical and Industrial Engineering Department, Abu Dhabi University, P.O. Box 59911, Abu Dhabi, United Arab Emirates

ARTICLE INFO

Keywords:
Cathode materials
Surface coating
Lithium conductivity
Lithium niobate
NCM811

ABSTRACT

Ni-rich oxides with layered structures are considered promising cathode materials for high-voltage lithium-ion batteries due to their high capacity and wide potential window. However, they suffer from volume expansion and contraction, as well as Ni reactivity with electrolyte components, leading to structural degradation and continuous lithium consumption during cycling. In this study, a highly electrically and ionically layer of Te-doped $LiNbO_3$ is coated onto the surface of $LiNi_{0.8}Co_{0.1}Mn_{0.1}O_2$ (NCM811) to protect the crystal structure from cracks and side reactions with the electrolyte at high voltages (4.3 V *vs.* Li/Li^+). Characterization techniques, including X-ray diffraction (XRD), dynamic light scattering (DLS), scanning electron microscopy (SEM), transmission electron microscopy (TEM), and electrochemical impedance spectroscopy (EIS), are employed to analyze the structure, morphology, and electrochemical performance of the coated materials. Results show that the delivered capacity at 0.1 C increases from 192.9 to 210.8 mAh g^{-1} and the capacity retention at 0.2 C increases from 79.7 to 89.2% after 100 cycles. Moreover, the diffusion coefficient of the coated NCM is 4.6×10^{-13} cm^2 s^{-1}, while that of bare NCM is only 1.5×10^{-13} cm^2 s^{-1} due to the reactivity of the coating layer with lithium. These findings provide valuable insights into the design and optimization of cathode materials for next-generation energy storage systems, contributing to the advancement of sustainable and efficient energy technologies.

1. Introduction

Lithium-ion batteries stand out as the most promising energy storage devices for electric vehicles and grid systems [1,2]. Commercial batteries typically employ graphite as an anode material due to its stable performance, moderate cost, and ease of processing, providing a capacity of 372 mAh g^{-1} [1]. However, the capacity of cathode materials remains limited, raising questions about their cyclability [3]. For instance, cathode materials like $LiFePO_4$ can store lithium through intercalation but have a theoretical capacity of only 170 mAh g^{-1}, which does not match that of graphite [3,4].

Another promising cathode material is lithium nickel cobalt manganese oxide (NCM), which offers a theoretical capacity exceeding 200 mAh g^{-1} [5,6]. Increasing the nickel content while decreasing cobalt and manganese ratios can yield higher capacity at a lower cost [7,8]. However, thermal stability and cycling life decrease due to the reduced role of cobalt in maintaining structural stability [7]. NCM materials are prone to cracking due to non-uniform volume expansion and contraction during cycling, leading to poor electrical conductivity and ongoing consumption of lithium ions to form a cathode electrolyte interface (CEI) layer [5,9].

Gas generation is another issue with NCM materials, stemming from the activation of oxygen anions due to the weakness of transition metals and oxygen [5,10,11]. Excess lithium, added during NCM synthesis to compensate for lithium evaporation at high temperatures, contributes to further gas release as it converts to lithium hydroxide and carbonate on the surface under ambient conditions [12,13]. The cation mixing between lithium ions and nickel ions leads to lower capacity and structure instability during cycling, causing severe fading [14–16]. These issues compromise structural stability and electrochemical performance, hindering the commercialization of nickel-rich NCM [13,17].

Various strategies have been employed to stabilize nickel-rich cathodes, including bulk material doping and surface coating [14,18–20]. Coating nickel-rich NCM surfaces protects the layered structure from atmospheric exposure and side reactions with electrolytes at high voltages [14,18]. Generally, coating materials can be categorized as either inactive, such as metal oxides, or active, like lithiated transition oxides [21–23]. Inactive coating layers isolate NCM from electrolytes to prevent side reactions and gas evaporation but impede lithium-ion movement during charge-discharge cycles, resulting in decreased capacity [9,24]. For example, coating layers

* Corresponding author.
E-mail address: mohammad.alkhedher@adu.ac.ae (M. Alkhedher).

https://doi.org/10.1016/j.nxener.2024.100216
Received 12 July 2024; Received in revised form 19 October 2024; Accepted 8 November 2024
2949-821X/© 2024 The Author(s). Published by Elsevier Ltd. This is an open access article under the CC BY-NC-ND license (http://creativecommons.org/licenses/by-nc-nd/4.0/).

containing Al_2O_3 and ZrO_2 enhance structural stability by reacting with electrolyte by-products like HF to form stable compounds AlF_3 and ZrF_4 [9,22,25].

In contrast, active coating layers serve multiple functions, including protecting active materials from electrolyte attack, stabilizing the crystal lattice, suppressing oxygen release, and enhancing lithium/electron conduction [9,11,26,27]. These properties improve capacity, cyclability, and the commercial viability of nickel-rich cathode materials [9,11,28]. Liu et al. converted lithium residue to lithium lanthanum titanium oxide (LLTO) on the surface of NCM, providing high lithium conductivity and structural stability, resulting in extended cyclability [26]. Sim et al. optimized the weight ratio of lithium tungsten oxide coating on NCM, achieving superior capacity retention of 85% over 80 cycles [28].

Lithium niobate ($LiNbO_3$), a solid electrolyte, exhibits low impedance due to high ionic conductivity and a layered structure [6]. It does not induce side reactions within the operational voltage range and can be synthesized through a simple process [6,29]. $LiNbO_3$ has been reported to enhance the interface between NCM811 and $Li_{10}GeP_2S_{12}$ solid electrolyte with just a 1 wt% coating [30]. Kong et al., created lithium vacancies by tungsten doping in the niobium site within $LiNbO_3$ perovskite, resulting in increased ionic conductivity to 1.75×10^{-6} S cm^{-1} at 90 ℃ [31]. However, $LiNbO_3$ exhibits poor electronic conductivity as a semiconductor, which can be addressed by doping to enhance electrical conductivity [32,33]. Recently, it has been demonstrated that the band gap of $LiNbO_3$ can be decreased from 3.5 eV for the pristine material to 0.9 eV after doping with tellurium (Te) [33].

In this study, polycrystalline NCM811 was synthesized via a calcination process, followed by coating with Te-doped $LiNbO_3$ for the first time. The coating layer exhibited significant improvement in lithium diffusion inside NCM cathode and improved the capacity retention and delivered capacity compared to undoped $LiNbO_3$. Scanning electron microscopy (SEM), transmission electron microscopy (TEM), and electrochemical performance confirmed that the coating layer effectively covered the NCM811 surface, addressing the limitations of NCM811 without compromising structure stability and electrochemical behavior.

2. Experimental section

2.1. Materials

All chemicals used were of analytical grade and used as received without further purification. Nickel acetate tetrahydrate ($Ni(OAc)_2.4H_2O$, Sigma-Aldrich), cobalt acetate tetrahydrate ($Co(OAc)_2.4H_2O$, Sigma-Aldrich), manganese acetate tetrahydrate ($Mn(OAc)_2.4H_2O$, Merck), absolute ethanol (C_2H_5OH, Aladdin Reagent), and lithium hydroxide ($LiOH.H_2O$, Thermo Scientific Chemicals) were used for preparing NCM811. Tellurium nitrate ($Te(NO_3)_4$, American Elements), ammonium citrate ($(NH_4)_2HC_6H_5O_7$, Fisher Scientific), ethylene glycol ($C_2H_6O_2$, Aladdin Reagent), ammonium niobate oxalate hydrate ($C_4H_4NNbO_9.xH_2O$) and lithium acetate (LiOAc) were used for coating NCM811 by Te-doped $LiNbO_3$.

2.2. Synthesis of Te-doped $LiNbO_3$ coated NCM811

NCM precursor with a molar ratio of Ni:Co:Mn = 8:1:1 was synthesized using hydrothermal method followed by calcination in an oxygen atmosphere. The stoichiometry ratio of $Ni(OAc)_2$, $Co(OAc)_2$, and $Mn(OAc)_2$ were dissolved in 50 mL ethanol by stirring for 2 h before heating in a Teflon-lined autoclave (100 mL) at 200 ℃ for 12 h. The resulting solid was separated by centrifugation, washed with excess deionized water (DI H_2O), and ethanol. The NCM precursor was then vacuum-dried at 50 ℃ for 24 h. The sample was ball-milled with a 10% excess of LiOH to compensate for lithium loss at high temperatures. A 2-step calcination process was carried out at 450 ℃ and 720 ℃ for 8 h and 12 h, respectively. After cooling, NCM811 was obtained and ground, and the obtained powder was referred to as NCM.

The coating process with Te-doped $LiNbO_3$ was performed as described in this literature [6]. Typically, 5 g of NCM was suspended in a mixture of ethylene glycol and DI water (1:1, *v:v*). Then, the stoichiometry ratio of $LiNbO_{2.9}Te_{0.1}$ precursors were dissolved, and the solution was vigorously stirred at 85 ℃ until drying. The resulting solid was sintered at 900 ℃ for 5 h to obtain Te-doped $LiNbO_3$-coated NCM811, hereafter referred to as NCM-TeLN. The coating layer accounts for 5 wt % of the NCM811.

2.3. Material characterizations

The X-ray diffraction (XRD) patterns of the as-prepared materials were collected by powder XRD (Rigaku D/max-2500 X-ray generator, 40 kV and 40 mA, Cu Kα wavelength), while the particle size distribution was measured by dynamic light scattering (DLS) method using a laser diffraction particle size analyzer (LA-950; HORIBA) after dispersion in ethanol. The morphology of NCM before and after coating was observed by scanning electron microscopy (FEI-Nova, Nano SEM430, 15 kV), with equipped with an energy dispersive X-ray analysis (EDS), while the thickness and uniformity of coating layer was observed by using a transmission electron microscope (TEM, Hitachi HT-7700, W-source, 100 kV). The chemical environment of elements was characterized by X-ray photoelectron spectroscopy (XPS, Scienta Omicron Multiprobe system) with a monochromatic beam size of 100 μm under an Al Kα X-ray source.

2.4. Electrochemical measurements

The working electrode consisted of 80% NCM, NCM-LN or NCM-TeLN as an active material, 10% carbon black as a conductive agent, and 10% Polyvinylidene difluoride as a binder, while NMP was used to adjust the viscosity. After casting on carbon-coated Al foil as a current collector, the sheet was dried at 80 ℃ in a vacuum oven for 24 h. The working electrode was punched with a thickness of 35 μm, surface area of 1.33 cm^2 and mass loading of around 3.2 mg cm^{-2}. Coin cells were assembled with the working electrode versus lithium metal as a reference and counter electrode. Around 1.0 M lithium bis(trifluoromethanesulfonyl)imide (LiTFSI) in ethylene carbonate (EC): diethyl carbonate (DEC), 1:1 vol% was utilized as electrolyte, while a 25 μm microporous polypropylene (PP) membrane (Celgard 2500) was used as a separator. All cells were aged for 12 h before measurements at room temperature to achieve better wettability and stable open circuit potential. The workstation potentiostat (CHI 660E, USA) was used to measure differential capacity (dQ/dV) at a range of 2.6–4.3 V (*vs.* Li/Li^+) at 0.1 C, where Q represents charge and V represents voltage. The delivered capacity and cycling performance were measured by galvanic charger NEWARE-BTS4000 (5 V), using the same potential range of dQ/dV.

Electrochemical impedance spectroscopy (EIS) was measured from the frequency range of 100 kHz to 10 mHz with an amplitude of 5 mV. Further analysis for EIS results were conducted to calculate the diffusion coefficient (D_{Li^+}) before and after coating using Eq. (1) as follows [34,35]:

$$D_{Li^+} = \frac{R^2T^2}{2A^2n^4F^4C^2\sigma^2} \quad (1)$$

where R is the constant gas, T is absolute temperature, A is area of working electrode, n is number of electron transfer during lithiation/delithaition, F is Faraday constant, C is molar concentration of lithium and σ is the Warburg factor. The latter was calculated by plotted the real impedance versus $\omega^{(-0.5)}$, as follows [34,35]:

$$Z_{re} = R + \sigma\omega^{-0.5} \quad (2)$$

where ω is the angular frequency at low frequency.

3. Results and discussion

3.1. Structure characterization and morphology

Various tools and techniques were employed to investigate the crystal structure and properties of NCM, NCM-LN and NCM-TeLN. The XRD pattern of NCM exhibited sharp, clear peaks at 2θ angles of 18.8, 36.7, 39.1, 39.3, 44.4, 48.9, 58.8, 64.5, 64.7, and 68.0, consistent with the NCM cathode material (JCPDS No. 09-0063) [25,36]. This indicates a rhombohedral structure with the $R\bar{3}m$ space group [14,36]. The significant splitting peaks (assigned by dash green line) at 2θ around 39° and 64.6° suggest that prepared materials possess a well-crystalline structure, facilitating lithium-ion diffusion during intercalation/deintercalation [19,37]. The coated samples with $LiNbO_3$ and Te-doped $LiNbO_3$ exhibited similar peaks to the uncoated one, indicating that the coating procedure at 900 ℃ maintained the layered structure of pristine NCM [19,37]. The absence of characteristic peaks for the coating layer is attributed to XRD limitations. No other peaks were observed, indicating that the methods used for synthesizing bare and coated NCM were successful in producing pure materials.

Rietveld refinement for XRD data for NCM, NCM-LN and NCM-TeLN was carried out as presented in Fig. S1 and Table S1. As seen, there are negligible changes in the lattice parameters (*a* and *c*) across the three samples, which suggest minimal structural impact from the coatings. The lattice parameters for the coated samples (NCM-LN and NCM-TeLN) are nearly identical to those of the uncoated NCM. This indicates that the coatings, including the Te-doped $LiNbO_3$, are not significantly altering the bulk structure of the NCM811 material. The unit cell volume (*V*) also remains very stable across the three samples, which suggests that any potential doping from the Te-doped $LiNbO_3$ coating has not led to significant lattice expansion or contraction in the NCM bulk. Additionally, no peak shifts were observed after coating, confirming no doping occurred in NCM crystals [16,23]. From this data, it seems that the Te-doped $LiNbO_3$ coating is not introducing significant doping inside the NCM811 structure, as the lattice parameters remain largely unchanged. Therefore, the refinement results support the conclusion that the coating serves more as a surface layer rather than altering the internal composition of the NCM material.

To assess the particle size distribution and the impact of the coating layer on the size of NCM, DLS tests were conducted as shown in Fig. 1b. The diameter of uncoated NCM particles ranged from 2 to 20 μm, and after coating, it increased to 30 μm. The relatively broad particle size distribution is beneficial for increasing the electrode density [38]. The D_{50} distribution of NCM, NCM-LN and NCM-TeLN is approximately 8.2, 10.1 and 10.3 μm, respectively. Such micro-scale size could result in less electrolyte and active material consumption to form a thin CEI, leading to high initial Coulombic efficiency (ICE) and long cyclability [25,38]. Furthermore, the $LiNbO_3$ coating layer effectively envelops the NCM particles, while the minimal alteration in the average particle size contributes to low impedance for lithium diffusion during the lithiation/delithiation process [39].

The micromorphology of pristine NCM is clearly visible in Fig. 2a, where the particles are spherical and well-dispersed without noticeable aggregation. Each spherical particle consists of agglomerated primary particles with internal porosity, as depicted in Fig. 2b. The different orientations of the grains lead to non-uniform lithiation insertion and extraction during the charge-discharge process, resulting in cracks and unstable CEI [18,37,40]. After coating with Te-doped $LiNbO_3$, the particles edges became smoother (Fig. 2c), while the coating layer connected the primary particles of polycrystalline NCM together and covered the pores, as shown in Fig. 2d. This improved contact may lead to enhanced lithiation homogeneity and reduced cracking during cycling, providing a longer cycle life [18,39,40].

The elemental distribution of NCM-TeLN was observed by Energy dispersive X-ray, as depicted in Fig. S2. The well-distributed nickel, cobalt, manganese, and oxygen are considered the constituents of polycrystalline NCM, while the presence of Nb originated from $LiNbO_3$ [40]. Additionally, tellurium signals were detected, indicating successful Te doping in the coating layer. It is anticipated that Te-doped $LiNbO_3$ could enhance the electronic conductivity of the coating layer, thereby providing rapid lithiation and delithiation process [33].

Further details about the morphology of NCM-TeLN were investigated by TEM. As shown in Fig. 3a, the NCM nanoparticles (44–46 nm) were interconnected to form dense polycrystalline secondary particles without any evident gaps, resulting from pore coverage by the coating layer. Moreover, the bulk surface of NCM with well-layered structures is visible in Fig. 3b, providing a favorable material for a rocking-chair battery. The thickness of the Te-doped $LiNbO_3$ coating layer was measured to be 6–7 nm, demonstrating uniformity in Fig. 3b. Such appropriate thickness not only inhibits cation mixing Li^+/Ni^{2+} and side reactions between NCM and the electrolyte but also does not impede lithium-ion movement [11,14,15,27]. In addition, the uniformity of the coating layer would provide uniform lithiation and delithiation process during cycling and different rates. This well-designed structure encouraged us to evaluate the electrochemical performance of lithium storage in the cathode material [15,27].

Surface analysis of NCM-TeLN was conducted using XPS to examine the oxidation states of various elements. The full survey in Fig. S3 shows distinct peaks for Te, Nb, O, and Li, confirming the chemical composition of the coating layer and the successful doping by Te. Additionally, the detection of Ni, Co, and Mn indicates the presence of NCM811. The high-resolution XPS spectra for Nb 3d and Te 3d in NCM-TeLN are shown in Figs. 3c and d, respectively. The Nb $3d_{3/2}$ and $3d_{5/2}$

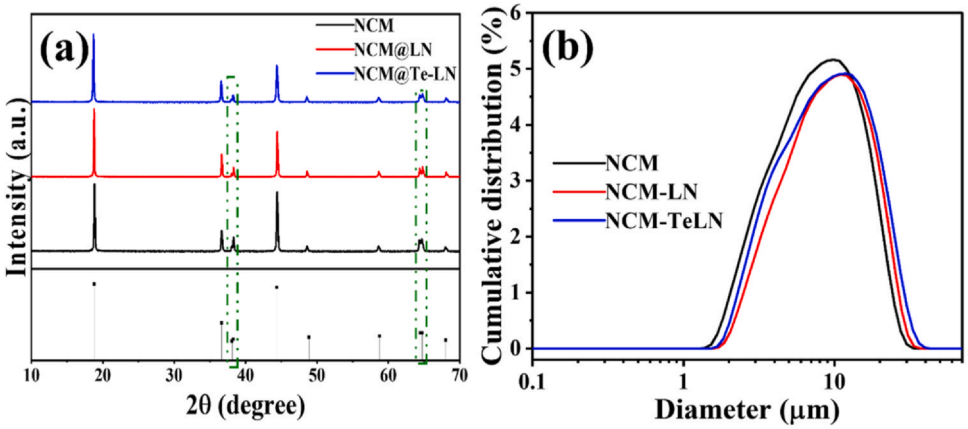

Fig. 1. (a) XRD patterns and (b) particle size distribution measured by dynamic light scattering (DLS) of NCM, NCM-LN and NCM-TeLN. NCM = lithium nickel cobalt manganese oxide; XRD = X-ray diffraction.

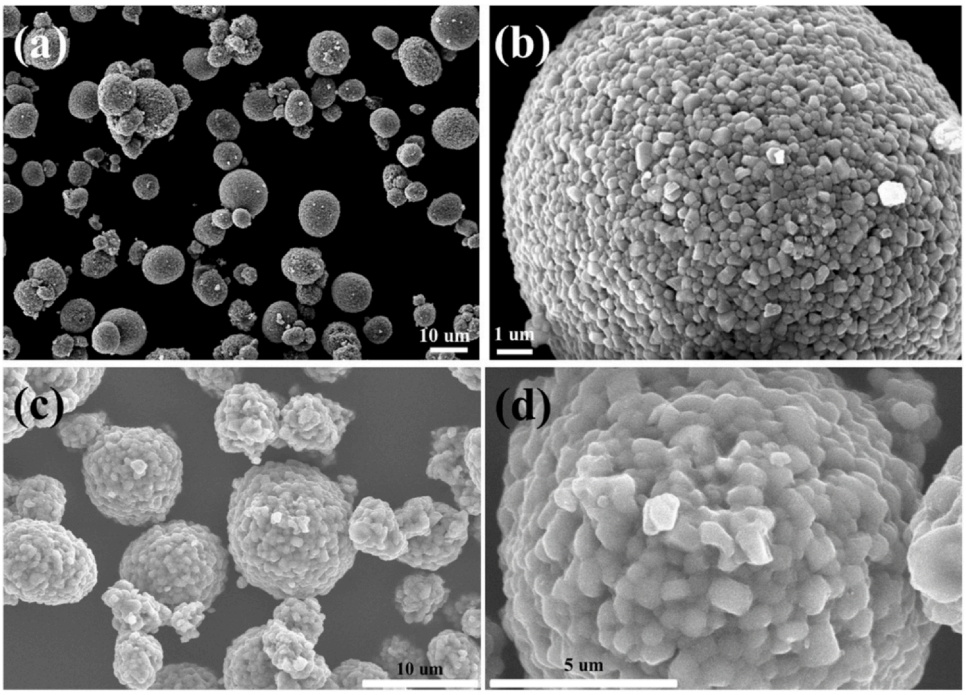

Fig. 2. SEM images of (a) NCM, (b) Magnified NCM, (c) NCM-TeLN, and (d) Magnified NCM-TeLN. NCM = lithium nickel cobalt manganese oxide; SEM = scanning electron microscopy.

peaks at 207.4 eV and 209.9 eV confirm that Nb is in the 5+ oxidation state, consistent with the Nb oxidation state in $LiNbO_3$ [29]. Similarly, the Te $3d_{3/2}$ and $3d_{5/2}$ peaks at 587.3 eV and 576.9 eV indicate that Te is in the 4+ oxidation state [41]. This difference in oxidation state could improve the internal electronic conductivity of the coating layer, and enhance the charge and discharge processes [33].

3.2. Electrochemical studies

The performance of NCM coated with Te-doped $LiNbO_3$ was investigated using various electrochemical techniques, including differential capacity, galvanic charge-discharge, and EIS, in comparison to the uncoated material.

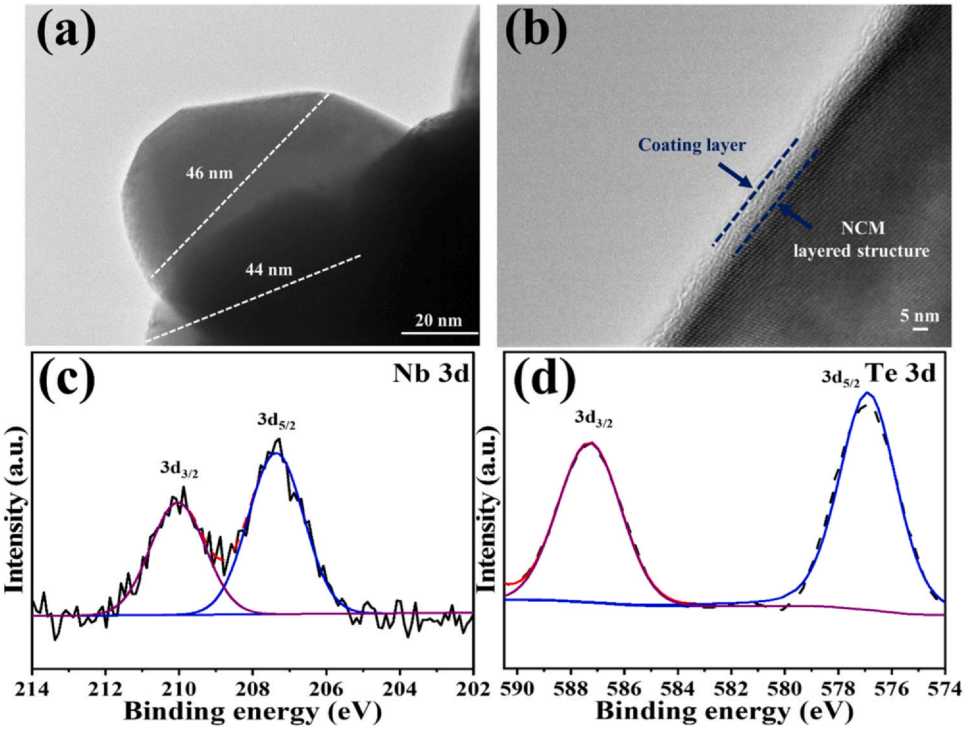

Fig. 3. TEM images of NCM-TeLN with scale bars of (a) 20 and (b) 5 nm, and high-resolution XPS spectra for (c) Nb 3d and (d) Te 3d of NCM-TeLN. NCM = lithium nickel cobalt manganese oxide; TEM = transmission electron microscopy; XPS = X-ray photoelectron spectroscopy.

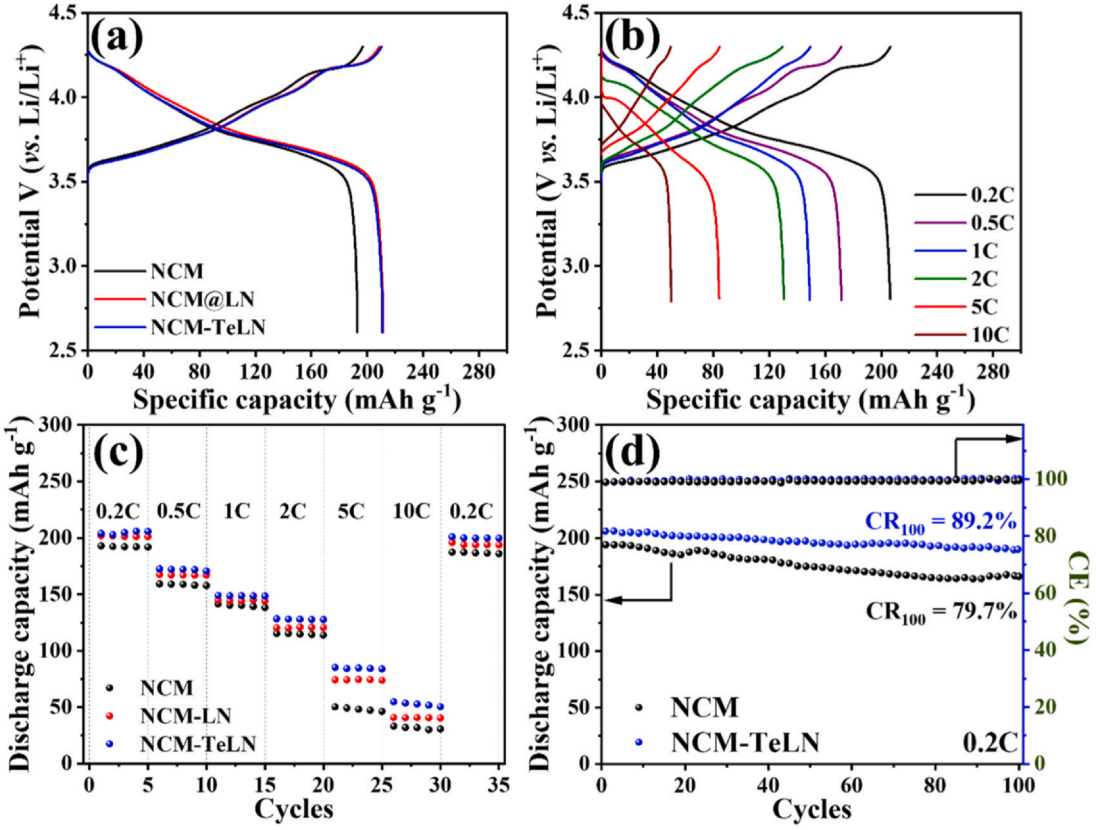

Fig. 4. (a) The GCD curves of first cycle of NCM, NCM-LN and NCM-TeLN at 0.1 C, (b) the GCD curves of NCM-TeLN from C-rates of 0.2 C to 10 C, (c) the corresponding delivered capacities at the same C-rate, and (d) cycling performance upon 100 cycles at a rate of 0.2 C after formation for three cycles at 0.1 C for NCM and NCM-TeLN. GCD = Galvanic charge-discharge; NCM = lithium nickel cobalt manganese oxide.

Differential capacity (dQ/dV) curves of NCM and NCM-TeLN showed 3 pairs of redox peaks during delithiation/lithiation, as presented in Figs. S4a and S4b, respectively. This indicates that the chemical compositions of the coating layer remain unchanged in the charging/discharging mechanism and that the thickness is appropriate for the cathode material without impeding lithium diffusion [36]. The broadening of the peaks is consistent with observations in other studies [29,42]. Additionally, smaller or non-uniform particles (Fig. 1b and Fig. 2) can create more heterogeneous lithium diffusion pathways, contributing to the broader dQ/dV peaks. Variations in particle morphology, grain boundaries, or defects in the crystal structure can also affect the electrochemical response, resulting in less distinct peaks. Since the test was conducted at a slower rate (0.1 C), lithium ions had more time to equilibrate within the material, further contributing to the broadening of the dQ/dV peaks. While sharper peaks may occur at higher cycling rates, such conditions may not reflect true equilibrium behavior of the system.

The first oxidation peak corresponds to the transition from the pristine hexagonal phase (H1) to the monoclinic phase (M) at 3.7 V (*vs.* Li/Li^+), while the second peak is related to the transition from the monoclinic phase (M) to the second hexagonal phase (H2) at 4.0 V (*vs.* Li/Li^+) [19,36]. The last transition occurs at a high voltage of 4.2 V (*vs.* Li/Li^+), indicating the transition from the second hexagonal phase (H2) to the third hexagonal phase (H3) [19,36]. These transitions are

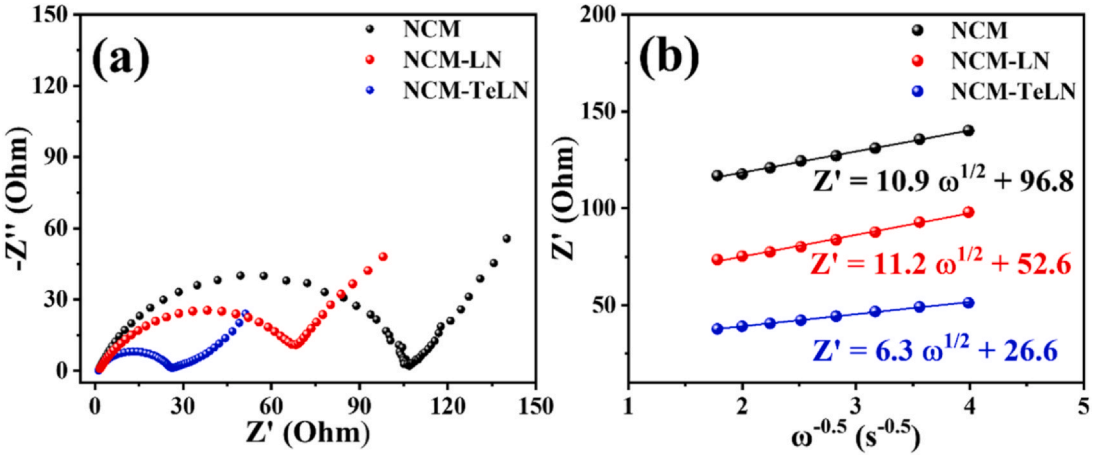

Fig. 5. (a) Nyquist plots of NCM, NCM-LN and NCM-TeLN and (b) the relation between real impedance and the $\omega^{-0.5}$ at low frequency. NCM = lithium nickel cobalt manganese oxide.

Table 1
Comparison of the electrochemical performance of $LiNbO_3$ coated NCM811 cathodes reported in literature

Coating layer	Rate/CR(%)@Cycles	Capacity (mAh g^{-1})@rate	Ref.
1 wt% $LiNbO_3$	0.5 C/93@100	200@0.1 C	[30]
1 wt% $LiNbO_3$	1 C/94@100	206@0.05 C	[29]
1 wt% $LiNbO_3$	1 C/90@200	194@0.1 C	[44]
TiO_2 Nanoparticles Assisted $LiNbO_3$	0.2 C/80@100	189@0.1 C	[42]
3 wt% $LiNbO_3$	1 C/87@200	204@0.1 C	[45]
Al_2O_3–$LiNbO_3$ co-coated	0.5 C/93@100	187@0.2 C	[46]
Te-Doped $LiNbO_3$	**0.2 C/89@100**	**211@0.1 C**	*This study*

CR = capacity retention; NCM = lithium nickel cobalt manganese oxide.

responsible for the degradation of the NCM structure; therefore, the intensity of these transitions decreases during cycling for uncoated NCM, as shown in Fig. S4a [14,19]. In contrast, the coated NCM maintains the same intensity for the first three cycles, as presented in Fig. S4b. This indicates that the coating layer of Te-doped $LiNbO_3$ improves the reversibility of the NCM structure from one phase to another, and it is expected that the coated NCM would provide better cycling retention [25,40].

Galvanic charge-discharge (GCD) measurements provide additional insights into the electrochemical performance under real-world operating conditions. Fig. 4a illustrates the discharge and charge profiles at 0.1 C for NCM coated with pristine $LiNbO_3$ and Te-doped $LiNbO_3$, compared to uncoated NCM. The voltage profiles and delivered capacities of the coated NCMs are similar, with both coatings showing higher capacities than uncoated NCM during the first cycle, attributable to the improved conductivity provided by the coatings. The coated NCM can charge and discharge within the range of 3.55–4.3 V (*vs.* Li/Li^+), with operation extending down to 2.6 V (*vs.* Li/Li^+) exhibiting additional plateaus. This suggests that the coatings effectively preserve the structural stability of NCM and do not induce side reactions within the operating voltage window [15,36]. Additionally, the ICE of both coated samples was 99.8%, compared to 97.9% for the uncoated NCM. This improvement is likely due to the role of the coating layer, which helps mitigate lithium loss from the NCM crystal structure by facilitating lithium ion migration [9,21].

Fig. 4b presents the GCD curves of the coated NCM starting from 0.2 C up to 10 C. As the rate increases, the charge curves at higher voltages become more linear, and the plateau at 4.2 V (*vs.* Li/Li^+) disappears. This indicates that the phase transition from H2 to H3 becomes less significant due to the faster charging rate [36]. Although the capacity decreases at higher rates, the elimination of the phase transition could improve the structural stability and cycling performance [25,36].

The corresponding delivered capacities of NCM-TeLN and NCM-LN compared to the uncoated NCM are shown in Fig. 4c. The reversible capacity of NCM-TeLN at 0.2 C, 0.5 C, 1 C, 2 C, 5 C, and 10 C was 205.8, 170.7, 148.5, 127.7, 83.5, and 50.5 mAh g^{-1}, respectively. These capacities are higher than those of the uncoated NCM. Notably, at lower rates, the capacities of NCM-TeLN were comparable to those of NCM-LN, but at higher rates, NCM-TeLN exhibited significantly higher capacities, while the uncoated NCM delivered 191.9 at 0.2 C and only 30.7 mAh g^{-1} at 10 C. This improvement in performance is likely due to enhanced phase transition properties, as observed in the dQ/dV test [25]. Additionally, the high electrical and ionic conductivity of the Te-doped $LiNbO_3$ coating facilitates the intercalation and de-intercalation processes. At 0.2 C, NCM-TeLN showed a capacity recovery of 199.8 mAh g^{-1}, retaining 97.1% of its capacity compared to the 5th cycle.

Fig. 4d and Fig. S5a illustrate the cycling performance of the as-prepared materials at 0.2 C over 100 cycles. Both coated and uncoated NCM samples exhibit a high Coulombic Efficiency (CE) of around 99% after an initial formation period of 3 cycles at 0.1 C. NCM-TeLN maintains a capacity retention of 89.2%, which is comparable to NCM-LN, while the uncoated NCM shows a lower capacity retention of 79.7%. Cycling tests conducted at 5 C, as shown in Fig. S5b, reveal significant differences among the samples. The coated samples, NCM-LN and NCM-TeLN, exhibit high-capacity retention (CR) of approximately 89% over 100 cycles. In contrast, the uncoated NCM only retains 37.8% of its capacity. This substantial improvement demonstrates that the coating layer significantly enhances the structural stability of NCM, reducing cracks and degradation during charge-discharge cycles and extending the cycling life [25,28]. This is attributed to the high chemical stability of Te-doped $LiNbO_3$ coating layer, which could shield the active materials from side reactions with the electrolyte [9,15,21]. Furthermore, the presence of Te dopant contributes to higher capacity retention at high rates due to improving the internal conductivity.

To investigate the effect of Te dopant in the coated layer on electrochemical performance and lithium diffusion, EIS measurements were conducted, as shown in Fig. 5a. Two different circuit fitting models (Fig. S6) were used to fit the EIS spectra for coated and uncoated NCM. For uncoated NCM, the bulk resistance (R_b) represents the resistance of the electrolyte, separator, and coin cell components [25,36]. Additionally, the charge transfer resistance (R_{ct}) and constant phase element (CPE_{ct}) denote the interface impedance between electrolyte and the active materials [25]. The Warburg (W) element was used to represent the diffusion behavior of lithium-ion inside the NCM [19,36]. For NCM-LN and NCM-TeLN, additional time-constant elements (R_{cl} and CPE_{cl}) were introduced to better fit the coating layer [22,29,43].

As indicated by the fitting values in Table S2, the R_{ct} decreased from 105.2 to 65.3 ohms after coating by pristine $LiNbO_3$ layer, which signifies an improvement in the charge transfer process due to enhanced interface interactions [30]. The incorporation of Te dopant into the $LiNbO_3$ layer further reduced R_{ct} to 24 ohms after coating, highlighting the increased conductivity facilitated by the Te dopant at the interface [22,36]. To assess the impact of the coating layer on ionic transport, the lithium-ion diffusion coefficient (D_{Li^+}) was calculated from the slope of real impedance versus $\omega^{-0.5}$ at low frequencies [35,43]. The lithium diffusion coefficient in NCM-TeLN was found to be 4.6×10^{-13} cm^2 s^{-1}, which is significantly higher than the coefficients for NCM and NCM-LN, which were 1.5×10^{-13} cm^2 s^{-1} and 1.4×10^{-13} cm^2 s^{-1}, respectively. This substantial increase in D_{Li^+}demonstrates that Te doping notably enhances lithium-ion conductivity compared to the pristine $LiNbO_3$ layer. The comparison between our study and other literature is presented in Table 1. As seen, Te-doped $LiNbO_3$ can significantly improve the capacity retention and delivered capacity. This significant improvement in lithium diffusion highlights the coating layer's effectiveness in accelerating charge carrier dynamics while concurrently protecting the NCM material [3,9,21,35].

4. Conclusions

In conclusion, the electrochemical performance of polycrystalline NCM has been significantly enhanced by coating it with a layer of Te-doped $LiNbO_3$, addressing key challenges associated with Ni-rich NCM811. The coating layer $LiNbO_3$ maintained the layered structure of NCM while providing additional protection against side reactions with the electrolyte and enhancing lithium-ion diffusion. The coated layer effectively bridged

the primary particles of NCM, reducing pore exposure and improving lithiation homogeneity. This resulted in better capacity retention and cycling stability. Electrochemical studies confirm the superiority of the coated NCM over the uncoated material. Differential capacity curves indicated that the coating layer did not alter the charging/discharging mechanism of NCM, indicating its inertness in the working potential and its compatibility with the electrode material. Galvanic charge-discharge tests show higher capacity and improved stability for the coated NCM, with reduced charge transfer resistance and maintained structural stability. Furthermore, EIS measurements demonstrated reduced charge transfer resistance and a significantly improved lithium-ion diffusion coefficient in the coated NCM by Te-doped $LiNbO_3$, reflecting enhanced electrochemical performance. Future research could focus on scaling up production processes and optimizing coating parameters to facilitate the commercialization of these advanced battery materials.

Declaration of Competing Interest

The authors declare the following financial interests/personal relationships which may be considered as potential competing interests: Mohammad Alkhedher reports financial support was provided by ASPIRE UAE. If there are other authors, they declare that they have no known competing financial interests or personal relationships that could have appeared to influence the work reported in this paper.

Acknowledgment

This research is supported by ASPIRE, the technology program management pillar of Abu Dhabi's Advanced Technology Research Council (ATRC), via the ASPIRE "VRI (Virtual Research Institute)".

Appendix A. Supporting material

Supplementary data associated with this article can be found in the online version at doi:10.1016/j.nxener.2024.100216.

References

[1] E. Strativnov, A. Khovavko, G. Nie, P.G. Ji, Graphite-graphene composite as an anode for lithium-ion batteries, Appl. Nanosci. 13 (2023) 7531–7536.
[2] M.M. Abdelaal, M. Alkhedher, Enhancing $Li_4Ti_5O_{12}$ anodes for high-performance batteries: Ti^{3+} induction via plasma-enhanced chemical vapor deposition and dual carbon/LLZO coatings, Batter. Supercaps. n/a e202400482.
[3] S. Zhao, Z. Guo, K. Yan, S. Wan, F. He, B. Sun, G. Wang, Towards high-energy-density lithium-ion batteries: strategies for developing high-capacity lithium-rich cathode materials, Energy Storage Mater. 34 (2021) 716–734.
[4] M.M. Abdelaal, M. Alkhedher, Dual optimization of $LiFePO_4$ cathode performance using manganese substitution and a hybrid lithiated Nafion-modified PEDOT:PSS coating layer for lithium-ion batteries, Electrochim. Acta 506 (2024) 145050.
[5] S. Chen, X. Zhang, M. Xia, K. Wei, L. Zhang, X. Zhang, Y. Cui, J. Shu, Issues and challenges of layered lithium nickel cobalt manganese oxides for lithium-ion batteries, J. Electroanal. Chem. 895 (2021) 115412.
[6] H. Yu, S. Wang, Y. Hu, G. He, L.Q. Bao, I.P. Parkin, H. Jiang, Lithium-conductive $LiNbO_3$ coated high-voltage $LiNi_{0.5}Co_{0.2}Mn_{0.3}O_2$ cathode with enhanced rate and cyclability, Green. Energy Environ. 7 (2022) 266–274.
[7] H. Pan, S. Jiao, Z. Xue, J. Zhang, X. Xu, L. Gan, Q. Li, Y. Liu, X. Yu, H. Li, The roles of Ni and Mn in the thermal stability of lithium-rich manganese-rich oxide cathode, Adv. Energy Mater. 13 (2023) 2203989.
[8] V. Gupta, M. Appleberry, W. Li, Z. Chen, Direct recycling industrialization of Li-ion batteries: the pre-processing barricade, Energy 2 (2024) 100091.
[9] J. Yan, H. Huang, J. Tong, W. Li, X. Liu, H. Zhang, H. Huang, W. Zhou, Recent progress on the modification of high nickel content NCM: coating, doping, and single crystallization, Interdiscip. Mater. 1 (2022) 330–353.
[10] C. Zhu, Y. Hu, N. Jiang, D. Pan, C. Li, Promoting reversible reaction of oxygen anions in cobalt-free lithium-rich layered oxides to improve their electrochemical performance, Appl. Surf. Sci. 566 (2021) 150587.
[11] L. Wang, G. Ding, Z. Yang, J. Chen, K. Liu, X. Huang, P. Lan, Y. Peng, S. Wang, Q. Zhao, Z. Yue, Y. Zhang, F. Sun, Synergistic construction of uniform $LiAlO_2$ coating on $LiNi_{0.8}Co_{0.1}Mn_{0.1}O_2$ cathode materials by acid etching and polyvinylpyrrolidone cross-linking approaches for high-performance Li-ion batteries, J. Alloy. Compd. 990 (2024) 174411.
[12] J. Välikangas, P. Laine, T. Hu, P. Tynjälä, M. Selent, P. Molaiyan, K. Jürgen, U. Lassi, Effect of secondary heat treatment after a washing on the electrochemical performance of Co-Free $LiNi_{0.975}Al_{0.025}O_2$ cathodes for Li-ion batteries, Small 20 (2024) 2305349.
[13] A.V. Ivanishchev, S.-H. Lee, J.-J. Kim, I.A. Ivanishcheva, S.-C. Nam, J.-H. Song, Li-ion diffusion characteristics of surface modified Ni-rich NCM cathode material, J. Electroanal. Chem. 932 (2023) 117242.
[14] F. Zhang, S. Lou, S. Li, Z. Yu, Q. Liu, A. Dai, C. Cao, M.F. Toney, M. Ge, X. Xiao, W.-K. Lee, Y. Yao, J. Deng, T. Liu, Y. Tang, G. Yin, J. Lu, D. Su, J. Wang, Surface regulation enables high stability of single-crystal lithium-ion cathodes at high voltage, Nat. Commun. 11 (2020) 3050.
[15] G. Cao, M. Zhang, L. Zhang, Y. Wang, Y. Yan, Z. Li, X. Sun, D. Zhang, Excellent high-rate cyclic performance of $LiNi_{0.8}Co_{0.1}Mn_{0.1}O_2$ cathodes via dual Li_2SiO_3/PPy coating, J. Alloy. Compd. 938 (2023) 168575.
[16] Y. Zhou, H. Zhang, Y. Wang, T. Wan, P. Guan, X. Zhou, X. Wang, Y. Chen, H. Shi, A. Dou, M. Su, R. Guo, Y. Liu, L. Dai, D. Chu, Relieving stress concentration through anion–cation codoping toward highly stable nickel-rich cathode, ACS Nano 17 (2023) 20621–20633.
[17] W. Yao, Y. Li, M. Olguin, S. Bai, M.A. Schroeder, W. Li, A. Liu, N.R. Park, B. Bhamwala, B. Sayahpour, G. Raghavendran, O. Borodin, M. Zhang, Y.S. Meng, Stabilizing high temperature operation and calendar life of $LiNi_{0.5}Mn_{1.5}O_4$, Energy 4 (2024) 100136.
[18] K. Mao, Y. Yao, Y. Chen, W. Li, X. Shen, J. Song, H. Chen, W. Luan, K. Wu, Fracture mechanisms of NCM polycrystalline particles in lithium-ion batteries: a review, J. Energy Storage 84 (2024) 110807.
[19] A. Yuan, H. Tang, L. Liu, J. Ying, L. Tan, L. Tan, R. Sun, High performance of phosphorus and fluorine co-doped $LiNi_{0.8}Co_{0.1}Mn_{0.1}O_2$ as a cathode material for lithium ion batteries, J. Alloy. Compd. 844 (2020) 156210.
[20] K. Huang, H. Yang, T. Xie, J. Zhou, T. Lan, S. Ong, H. Jiang, Y. Zeng, L. Wan, H. Guo, Y. Zhang, $Li_4Ti_5O_{12}$-TiO_2 composite coating layer enabling $LiNi_{0.8}Co_{0.1}Mn_{0.1}O_2$ electrodes with superior cycling performance, J. Electroanal. Chem. 951 (2023) 117923.
[21] M. Akhilash, P. Salini, B. John, S. Sujatha, T. Mercy, Surface modification on nickel rich cathode materials for lithium-ion cells: a mini review, Chem. Rec. 23 (2023) e202300132.
[22] J. Wang, D. Zhao, G. Zhou, S. Wei, S. Hou, Y. Li, H. Ma, Y. Yuan, X. Yan, X. Hou, Effects of Al_2O_3 and $LiAlO_2$ Co-coating on electrochemical properties of $LiNi_{0.8}Co_{0.1}Mn_{0.1}O_2$ cathode materials, Ceram. Int. 49 (2023) 15842–15850.
[23] X. Qu, H. Huang, T. Wan, L. Hu, Z. Yu, Y. Liu, A. Dou, Y. Zhou, M. Su, X. Peng, H.-H. Wu, T. Wu, D. Chu, An integrated surface coating strategy to enhance the electrochemical performance of nickel-rich layered cathodes, Nano Energy 91 (2022) 106665.
[24] Y. Liu, T. Zeng, G. Li, T. Wan, M. Li, X. Zhang, M. Li, M. Su, A. Dou, W. Zeng, Y. Zhou, R. Guo, D. Chu, The surface double-coupling on single-crystal $LiNi_{0.8}Co_{0.1}Mn_{0.1}O_2$ for inhibiting the formation of intragranular cracks and oxygen vacancies, Energy Storage Mater. 52 (2022) 534–546.
[25] Y. Hou, Y. Ren, T. Shi, J. Li, H. Li, L. Zhang, Y. Liu, Y. Wan, S. Zhang, D. Zhu, The surface Al_2O_3 coating and bulk Zr doping drastically improve the voltage fade and cycling stability of $Li(Ni_{0.8}Mn_{0.1}Co_{0.1})O_2$ cathode materials, J. Alloy. Compd. 939 (2023) 168778.
[26] S. Liu, C. Zhang, Q. Su, L. Li, J. Su, T. Huang, Y. Chen, A. Yu, Enhancing electrochemical performance of $LiNi_{0.6}Co_{0.2}Mn_{0.2}O_2$ by lithium-ion conductor surface modification, Electrochim. Acta 224 (2017) 171–177.
[27] B. Xiao, D. Li, X. Dai, Y. Wei, Y. Liao, C. Wang, F. Ji, F. Wu, Construction of a robust lithium cobalt phosphate layer for enhancement of the electrochemical performance of $LiNi_{0.8}Co_{0.1}Mn_{0.1}O_2$ at high voltage, Electrochim. Acta 475 (2024) 143648.
[28] S.-J. Sim, S.-H. Lee, B.-S. Jin, H.-S. Kim, Effects of lithium tungsten oxide coating on $LiNi_{0.90}Co_{0.05}Mn_{0.05}O_2$ cathode material for lithium-ion batteries, J. Power Sources 481 (2021) 229037.
[29] P. He, M. Zhang, J. Wu, Y. Li, Y. Wang, Y. Yan, D. Zhang, X. Sun, Enhanced cyclic stability and discharge capacity of NCM811 cathode by coating ferroelectric-type $LiNbO_3$ ionically conductive layer, J. Alloy. Compd. 967 (2023) 171822.
[30] X. Li, L. Jin, D. Song, H. Zhang, X. Shi, Z. Wang, L. Zhang, L. Zhu, $LiNbO_3$-coated $LiNi_{0.8}Co_{0.1}Mn_{0.1}O_2$ cathode with high discharge capacity and rate performance for all-solid-state lithium battery, J. Energy Chem. 40 (2020) 39–45.
[31] L. Xian, J. Peng, L.-B. Kong, Improved ion transport capacity in ceramic $LiNbO_3$ by doping with W to increase the Li vacancies, J. Solid State Electrochem. 28 (2024) 3221–3230.
[32] C. Godau, T. Kämpfe, A. Thiessen, L.M. Eng, A. Haußmann, Enhancing the domain wall conductivity in lithium niobate single crystals, ACS Nano 11 (2017) 4816–4824.
[33] I. Ait Brahim, N. Bekkioui, M. Tahiri, H. Ez-Zahraouy, Doping effect of chalcogens on electronic and optical properties of perovskite $LiNbO_3$ compound: Ab initio calculations, Chem. Phys. 550 (2021) 111320.
[34] H. Raj, A. Sil, PEDOT:PSS coating on pristine and carbon coated $LiFePO_4$ by one-step process: the study of electrochemical performance, J. Mater. Sci.: Mater. Electron. 30 (2019) 13604–13616.
[35] M.-d Zhu, H.-l Zhu, J.-m Guo, C.-c Lu, Y. Ji, J. Hu, X.-x Tan, Z.-y Chen, Enhanced rate capability and cycling stability of conductive oxide-coated $LiNi_{0.8}Co_{0.1}Mn_{0.1}O_2$ for lithium-ion batteries, Ionics 29 (2023) 1711–1720.
[36] S. She, Y. Zhou, Z. Hong, Y. Huang, Y. Wu, Surface coating of NCM-811 cathode materials with g-C_3N_4 for enhanced electrochemical performance, ACS Omega 7 (2022) 24851–24857.
[37] Y. Gao, X. Wang, Z. Zou, J. Geng, M. Chen, F. Yu, Enhanced electrochemical performance of LiV_2O_4-coated and V^{4+}-doped $LiNi_{0.8}Co_{0.1}Mn_{0.1}O_2$ cathode for lithium-ion batteries, J. Mater. Sci.: Mater. Electron. 34 (2023) 1448.
[38] W. Zhao, L. Zou, L. Zhang, X. Fan, H. Zhang, F. Pagani, E. Brack, L. Seidl, X. Ou, K. Egorov, X. Guo, G. Hu, S. Trabesinger, C. Wang, C. Battaglia, Assessing long-term cycling stability of single-crystal versus polycrystalline nickel-rich NCM in pouch cells with 6 mAh cm^{-2} electrodes, Small 18 (2022) 2107357.

[39] S. Yuan, H. Yu, T. Zhou, R. Liang, G. Jiang, J. Xiong, A. Zheng, K. Li, X. Wang, Preparation and electrochemical performance of La_2O_3 coated $LiNi_{0.8}Co_{0.1}Mn_{0.1}O_2$ material, Int. J. Electrochem. Sci. 18 (2023) 100141.
[40] G. Zha, W. Hu, S. Agarwal, C. Ouyang, N. Hu, H. Hou, High performance layered $LiNi_{0.8}Co_{0.07}Fe_{0.03}Mn_{0.1}O_2$ cathode materials for Li-ion battery, Chem. Eng. J. 409 (2021) 128343.
[41] X. Chen, Y. Pan, Y. Ding, H. Lian, J. Lin, L. Li, Enhanced Efficiency, broadened excitation, and tailored Er^{3+} luminescence triggered by Te^{4+} codoping in $Cs_2NaYbCl_6$ crystals for multifunctional applications, Inorg. Chem. 63 (2024) 3525–3534.
[42] X. Bai, P. Wang, J. Zhang, J. Li, TiO_2 Nanoparticles assisted $LiNbO_3$-coated $LiNi_{0.8}Co_{0.1}Mn_{0.1}O_2$ cathode for lithium-ion batteries, ACS Appl. Nano Mater. 7 (2024) 2753–2763.
[43] X. Lu, Q. Mao, Y. Wang, T. Ji, Y. Zeng, Y. Xu, Y. Xia, R. Shan, P. Xu, Y. Cai, J. Yao, Effect of lithium to zirconium ratio on microstructure and electrochemical performances of LZO modified $LiNi_{0.8}Co_{0.1}Mn_{0.1}O_2$ cathode materials, Surf. Interfaces 36 (2023) 102480.
[44] G. Hu, Y. Tao, Y. Lu, J. Fan, L. Li, J. Xia, Y. Huang, Z. Zhang, H. Su, Y. Cao, Enhanced electrochemical properties of $LiNi_{0.8}Co_{0.1}Mn_{0.1}O_2$ cathode materials modified with lithium-ion conductive coating $LiNbO_3$, ChemElectroChem 6 (2019) 4773–4780.
[45] Z. Li, Y. You, Y. Liu, J. Liu, J. Peng, M. Yuan, Analyzing the mechanism of performance improvement in $LiNi_{0.8}Co_{0.1}Mn_{0.1}O_2$ through coating with $LiNbO_3$ fast ion conductor, Ceram. Int. 50 (2024) 30493–30503.
[46] C.N. Thi Linh, V.D. Thuc, D.D. Mai, M.C. Nguyen, M.A. Le, D.T. Pham, W.J. Yu, D. Kim, High structural stability and Li-conduction of $LiNi_{0.8}Co_{0.1}Mn_{0.1}O_2$ cathode co-coated by Al_2O_3 and $LiNbO_3$ for high performance lithium-ion battery, J. Mater. Chem. A 12 (2024) 27610–27622.